Cross-well electromagnetic imaging in three dimensions

Michael S. Zhdanov[1]   **Ken Yoshioka**[2]

Key Words: cross-well, three-dimensional, tomography, electromagnetic, localized quasi-linear approximation, grouping

ABSTRACT

In this paper, we develop a new technique for 3D cross-well electromagnetic tomography, based on an EM borehole survey consisting of a moving vertical magnetic dipole transmitter, located in one or several boreholes, and a tri-axial induction receiver, located in the other boreholes. The method is based on the LQL approximation for forward modelling, which results in a fast inversion scheme. The method incorporates both a smooth regularized inversion, which generates a smooth image of the inverted resistivity, and a focusing regularized inversion, producing a sharp focused image of the geoelectrical target. The practical application of the method to synthetic data demonstrates its ability to recover the resistivity, location, and shape of resistive and conductive rock formations.

INTRODUCTION

Cross-well electromagnetic surveys are used both in petroleum exploration for reservoir study and in mineral exploration for the delineation of massive sulphide mineralization. Over the last decade, significant progress has been made in developing sophisticated methods of cross-well electromagnetic imaging and inversion (Wilt et al., 1995; Alumbaugh and Morrison, 1995; Newman, 1995; Alumbaugh and Newman, 1997; Zhou and Greenhalgh, 2002). However, 3D cross-well imaging is still a very challenging problem. The main difficulties in the solution of this problem are related to the fact that for cross-well EM imaging we usually use a multi-transmitter observation system. This observation system requires multiple modelling and inversion for every position of the transmitter, which is very time consuming. In this paper, we overcome this difficulty by applying a new technique for inversion of 3D cross-well electromagnetic data using the localized quasi-linear (LQL) approximation for forward modelling and focusing inversion (Zhdanov, 2002). This technique represents a novel approach to cross-well electromagnetic tomographic imaging.

[1]   *University of Utah*
Department of Geology and Geophysics
135 South 1460 East, Rm 719
Salt Lake City, UT, 84112
U. S. A.
Tel: +1 (801) 581-7750
Fax: +1 (801) 581-2062
Email: mzhdanov@mines.utah.edu

[2]   *Ken Yoshioka*
University of Utah
Department of Geology and Geophysics
135 South 1460 East, Rm 719
Salt Lake City, UT, 84112
U. S. A.
Tel: +1 (801) 585-5461
Fax: +1 (801) 581-7065
Email: yoshioka@mines.utah.edu

The quasi-linear approximation has proven to be a powerful tool in electromagnetic forward modelling. It is based on the assumption that the anomalous electric field within an inhomogeneous domain is linearly proportional to the background (normal) field through an electrical reflectivity tensor. In the original formulation of the quasi-linear approximation (Zhdanov and Fang, 1996a, b), this tensor was determined by solving a minimisation problem based on an integral equation for the scattering currents. However, the electrical reflectivity tensor depends on the illuminating (background) field. In other words, for any new position of the transmitter we have to recalculate the tensor coefficient anew. This slows down the calculations for arrays of sources, which are typical for many geophysical applications, for example for cross-well tomography, or for well-logging modelling and inversion. In this paper, we use a new approach to quasi-linear approximation based on a so-called localized electrical reflectivity tensor that is independent of the source position (Zhdanov and Tartaras, 2002). We introduce a new approach to interpretation of the cross-well EM data, which we call "grouping". In the framework of this approach, we divide all transmitters and receivers into a number of groups, and determine the material property parameter and electrical reflectivity coefficient independently for each group of transmitters and receivers. We develop a new, fast 3D EM inversion method using the LQL approximation with grouping.

In the numerical inversion code, we implement options for focusing or for smooth regularized inversion. The traditional inversion methods are usually based on Tikhonov regularization theory, which provides a stable solution of the inverse problem (Tikhonov and Arsenin, 1977). This goal is reached, as a rule, by introducing a maximum smoothness stabilising functional. The solution obtained provides a smooth image, which in many practical situations, especially in mineral exploration, does not describe properly the mining target. In cross-well imaging, we apply a different way of regularized inversion using a specially selected stabilising functional that minimises the volume where strong model parameter variations and discontinuities occur (Portniaguine and Zhdanov, 1999; Zhdanov, 2002). We demonstrate that focusing regularization helps to generate a stable solution to the cross-well EM imaging problem, and produces a more "focused" image of underground structures than conventional methods. The numerical examples demonstrate the effectiveness of this technique in 3D cross-well electromagnetic data interpretation for imaging both conductive and resistive targets.

CROSS-WELL EM TOMOGRAPHIC IMAGING BASED ON THE LOCALIZED QUASI-LINEAR APPROXIMATION

We consider a case of cross-well electromagnetic (EM) tomography, based on an EM borehole survey consisting of a moving vertical magnetic dipole transmitter, located in one or several boreholes, and a tri-axial induction receiver, located in the other boreholes. The transmitter generates a frequency-domain EM field. The receivers measure three magnetic field components H_x, H_y, and H_z. The goal is to reconstruct the three-dimensional conductivity distribution in some anomalous area D between two

boreholes, assuming that the background σ_b can be represented by the known horizontally layered conductivity.

In the framework of the integral equation (IE) numerical modelling method, the anomalous electric field $\mathbf{E}^a$ and magnetic field $\mathbf{H}^a$, due to a 3D inclusion with anomalous conductivity $\Delta\sigma$, located between the boreholes in a layered background, are given as an integral of the anomalous conductivity and the total electric field over the anomalous domain D:

$$\mathbf{E}^a(\mathbf{r}_j) = \iiint_D \hat{\mathbf{G}}_E(\mathbf{r}_j|\mathbf{r}) \cdot \Delta\sigma \left[\mathbf{E}^b(\mathbf{r}) + \mathbf{E}^a(\mathbf{r})\right] dv ,$$
$$= \mathbf{G}_E\left[\Delta\sigma\left(\mathbf{E}^b + \mathbf{E}^a\right)\right] \tag{1}$$

$$H^a(\mathbf{r}_j) = \iiint_D \hat{\mathbf{G}}_H(\mathbf{r}_j|\mathbf{r}) \cdot \Delta\sigma \left[\mathbf{E}^b(\mathbf{r}) + \mathbf{E}^a(\mathbf{r})\right] dv ,$$
$$= \mathbf{G}_H\left[\Delta\sigma\left(\mathbf{E}^b + \mathbf{E}^a\right)\right] \tag{2}$$

where $\hat{\mathbf{G}}_E(\mathbf{r}_j|\mathbf{r})$ and $\hat{\mathbf{G}}_H(\mathbf{r}_j|\mathbf{r})$ are the electric and magnetic Green's tensors defined for an unbounded conductive medium with the background conductivity σ_b; $\mathbf{G}_E$ and $\mathbf{G}_H$ are corresponding Green's linear operators. The background electric field $\mathbf{E}^b$ is generated by the given transmitters in the model with a background distribution of conductivity σ_b. Our goal is to find the anomalous conductivity from the measurements of the anomalous magnetic field obtained by the moving tri-axial induction tool.

In the framework of the LQL approximation, we assume that the anomalous electric field inside the anomalous domain is linearly proportional to the background electric field through an electrical reflectivity coefficient λ_I,

$$\mathbf{E}_I^a(\mathbf{r}) = \lambda_I(\mathbf{r})\mathbf{E}_I^b(\mathbf{r}) , \tag{3}$$

where I is the index of the transmitters. Thus, for different transmitter positions we have, in general, different reflectivity coefficients λ_I.

Substituting equation (3) back into equations (1) and (2), we find

$$\mathbf{E}_{QL_I}^a(\mathbf{r}) = \mathbf{G}_E\left[\Delta\sigma(1 + \lambda_I)\mathbf{E}_I^b\right] , \tag{4}$$

$$\mathbf{H}_{QL_I}^a(\mathbf{r}) = \mathbf{G}_H\left[\Delta\sigma(1 + \lambda_I)\mathbf{E}_I^b\right] . \tag{5}$$

Inside the anomalous domain D, the QL approximation for the anomalous field should satisfy equation (3). Substituting this equation into equation (4), we find

$$\lambda_I(\mathbf{r})\mathbf{E}_{QL_I}^b(\mathbf{r}) = \mathbf{G}_E\left[\Delta\sigma(1 + \lambda_I)\mathbf{E}_I^b\right], \quad \mathbf{r} \in D, \quad I = 1, 2, \ldots, N . \tag{6}$$

Let us calculate the average values of the left-hand and right-hand sides of equation (6), taking into account that $\mathbf{G}_E$ is a linear operator:

$$\frac{1}{N}\sum_{I=1}^{N}\lambda_I(\mathbf{r})\mathbf{E}_I^b(\mathbf{r}) = \mathbf{G}_E\left\{\Delta\sigma\left[\frac{1}{N}\sum_{I=1}^{N}\mathbf{E}_I^b(\mathbf{r}) + \frac{1}{N}\sum_{I=1}^{N}\lambda_I(\mathbf{r})\mathbf{E}_I^b(\mathbf{r})\right]\right\} . \tag{7}$$

We can introduce the *mean value reflectivity coefficient* λ_M according to the formula

$$\frac{1}{N}\sum_{I=1}^{N}\lambda_I(\mathbf{r})\mathbf{E}_I^b(\mathbf{r}) = \lambda_M(\mathbf{r})\frac{1}{N}\sum_{I=1}^{N}\mathbf{E}_I^b(\mathbf{r}) = \lambda_M(\mathbf{r})\tilde{\mathbf{E}}^b(\mathbf{r}) . \tag{8}$$

where

$$\tilde{\mathbf{E}}^b(\mathbf{r}) = \frac{1}{N}\sum_{I=1}^{N}\mathbf{E}_I^b(\mathbf{r}) \tag{9}$$

is the averaged background field. Using these notations, equation (7) takes the form

$$\lambda_M(\mathbf{r})\tilde{\mathbf{E}}^b(\mathbf{r}) = \mathbf{G}_E\left[\Delta\sigma(1 + \lambda_M)\tilde{\mathbf{E}}^b\right] . \tag{10}$$

We assume now that the anomalous parts of the electric, $\mathbf{E}_I^a(\mathbf{r}_j)$, and/or magnetic, $\mathbf{H}_I^a(\mathbf{r}_j)$, fields are measured at a number of observation points, $\mathbf{r}_j$. Using the LQL approximation for the observed fields, $\mathbf{d}_I$, we arrive at the following equation:

$$\mathbf{d}_I(\mathbf{r}_j) = \mathbf{G}_d\left[\Delta\sigma(1 + \lambda_I)\mathbf{E}_I^b\right] , \tag{11}$$

where $\mathbf{d}_I$ stands for the electric or magnetic field, $\mathbf{E}$ or $\mathbf{H}$, and $\mathbf{G}_d$ denotes operator $\mathbf{G}_E$ or $\mathbf{G}_H$ correspondingly. We now calculate the average values of the left-hand and right-hand sides of equation (11), taking into account that $\mathbf{G}_d$ is a linear operator:

$$\tilde{\mathbf{d}}(\mathbf{r}_j) = \mathbf{G}_d\left\{\Delta\sigma\left[\frac{1}{N}\sum_{I=1}^{N}\mathbf{E}_I^b(\mathbf{r}) + \frac{1}{N}\sum_{I=1}^{N}\lambda_I(\mathbf{r})\mathbf{E}_I^b(\mathbf{r})\right]\right\} ,$$
$$= \mathbf{G}_d\left[\Delta\sigma(1 + \lambda_M)\tilde{\mathbf{E}}^b\right] \tag{12}$$

where $\tilde{\mathbf{d}}$ stands for the averaged observed data:

$$\tilde{\mathbf{d}}(\mathbf{r}_j) = \frac{1}{N}\sum_{I=1}^{N}\mathbf{d}_I(\mathbf{r}_j) .$$

Following Zhdanov and Fang (1996a) and Zhdanov and Fang (1999), we introduce a new function,

$$m(\mathbf{r}) = \Delta\sigma(\mathbf{r})(1 + \lambda_M(\mathbf{r})) . \tag{13}$$

Substituting equation (13) into equation (12), we arrive at the following equation

$$\tilde{\mathbf{d}}(\mathbf{r}_j) = \mathbf{G}_d\left(m(\mathbf{r})\tilde{\mathbf{E}}^b(\mathbf{r})\right) , \tag{14}$$

which is linear with respect to the material property parameter $m(\mathbf{r})$.

We can consider now a new inverse problem, with respect to the parameter m, represented by equation (14), which is a linear problem. Note that this linear problem is formulated for all possible transmitter and receiver positions simultaneously! Thus, by using the LQL approximation we arrive at one linear inverse problem for the entire observation array.

This linear problem is solved by using the re-weighted conjugate method with image focusing. The focusing algorithm is based on application of a special stabilising functional, which minimises the volume where strong model parameter variations and discontinuities occur. As a result, we can reconstruct a geoelectrical model with sharp boundaries between different rock formations. More details about this approach can be found in the monograph on inversion theory by Zhdanov (2002).
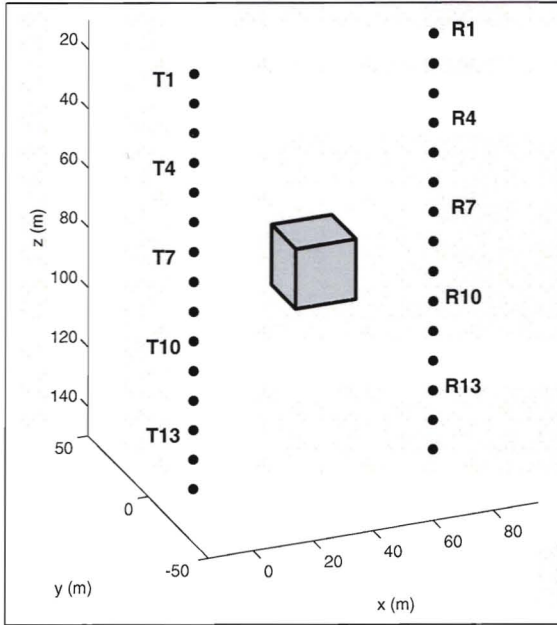
Fig. 1. Model 1, representing a cubic conductive body with resistivity of 1 ohm.m in a 100 ohm.m homogeneous background. The electromagnetic field in the model is generated by a vertical magnetic dipole transmitter moving vertically along the left borehole and transmitting a signal every 10 metres. The tri-axial magnetic component receivers are located along the right borehole, deployed in the z-direction with 10-m separation.

According to equation (10), after determining parameter m we can find the electrical reflectivity coefficient λ_M as the solution of the following minimisation problem:

$$\left\| \lambda_M(\mathbf{r})\widetilde{\mathbf{E}}^b(\mathbf{r}) - \mathbf{G}_E\big(m(\mathbf{r})\widetilde{\mathbf{E}}^b\big) \right\|^2 = \min \quad . \tag{15}$$

Finally, we find $\Delta\sigma$ from equation (13).

Note that, in a practical implementation of this method for the inversion of multi-transmitter and multi-receiver data, we can use the "grouping" approach. In the framework of this approach, we divide all transmitters and receivers into a number of groups and determine the material property parameter and electrical reflectivity coefficient independently for each group of transmitters and receivers. This technique is helpful in a situation where the different groups of the transmitters illuminate the geoelectrical target from different directions. In this case, the averaging outlined by equations (6) and (12) should be conducted only within each group. As a result, equation (14) should be written now separately for each group:

$$\widetilde{\mathbf{d}}_g(\mathbf{r}_j) = \mathbf{G}_d\big(m_g(\mathbf{r})\widetilde{\mathbf{E}}_g^b(\mathbf{r})\big), g = 1, 2, ..., G \quad , \tag{16}$$

where

$$\widetilde{\mathbf{d}}_g(\mathbf{r}_j) = \frac{1}{N_g}\sum_{I_g=1}^{N_g}\mathbf{d}_{I_g}(\mathbf{r}_j) \quad ,$$

and

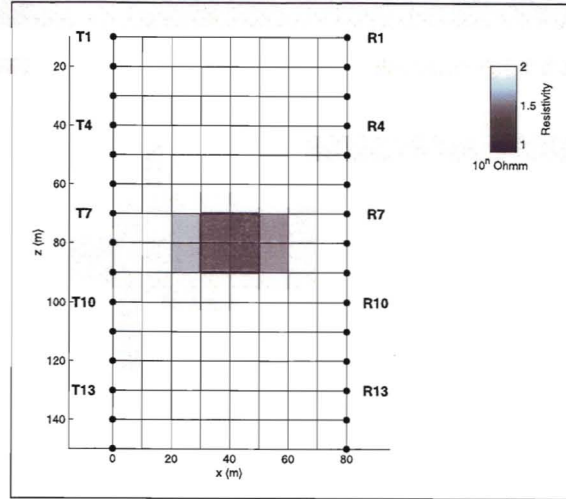$$\widetilde{\mathbf{E}}_g^b(\mathbf{r}) = \frac{1}{N_g}\sum_{I=1}^{N_g}\mathbf{E}_{I_g}^b(\mathbf{r}) \quad .$$

Fig. 2. A vertical cross section between two boreholes of the model obtained as a result of focusing inversion of the cross-well tomographic data for Model 1.
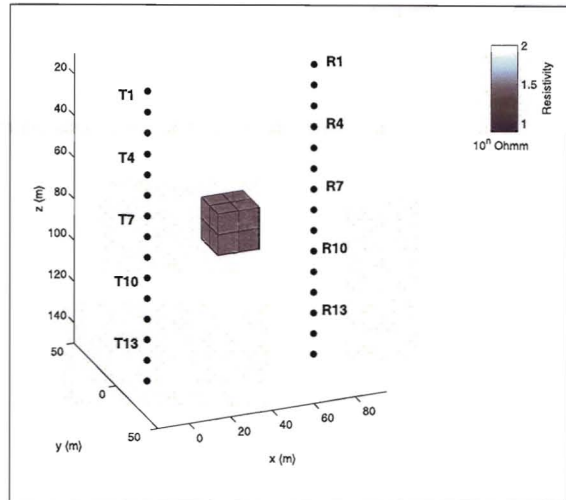

Fig. 3. A 3D view of the inversion result for Model 1 with volume rendering. The cut-off level for this image is 20 ohm.m. This means that only the cells with a value of resistivity less than 20 ohm.m are displayed.

In the last equations, G is the number of groups, N_g is the number of transmitters within the corresponding group, and $m_g(\mathbf{r})$ is a material property parameter for a given group.

The reflectivity coefficient λ_{M_g} is determined now for each group independently, from the equation

$$\left\| \lambda_{M_g}(\mathbf{r})\widetilde{\mathbf{E}}_g^b(\mathbf{r}) - \mathbf{G}_E\big(m_g(\mathbf{r})\widetilde{\mathbf{E}}_g^b(\mathbf{r})\big) \right\|^2 = \min, g = 1, 2, ..., G \quad , \tag{17}$$

The final anomalous conductivity distribution is found as a solution of the least squares problem

$$\sum_{g=1}^{G}\left\| m_g(\mathbf{r}) - \Delta\sigma(\mathbf{r})\big(1 + \lambda_{M_g}(\mathbf{r})\big) \right\|^2 = \min \quad . \tag{18}$$
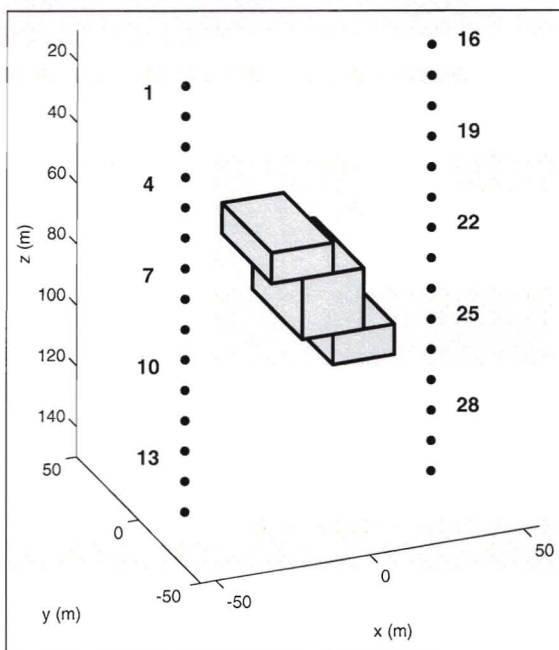
Fig. 4. Model 2, of a dipping conductive body with resistivity 10 ohm.m in a 100 ohm.m homogeneous background. The EM field in this model is generated by vertical magnetic transmitters successively located in each borehole (the transmitter locations are shown by the bold dots with the numbers). The data are recorded by two sets of receivers in the left and right boreholes.

NUMERICAL MODELLING RESULTS

We generated synthetic EM data for typical geoelectrical models of conductive or resistive targets within a homogeneous background. Model 1 represents a cubic conductive body with resistivity of 1 ohm.m in a 100 ohm.m homogeneous background (Figure 1). The body is located at the centre between two boreholes. The body sides in the x, y, and z directions have a length of 20 m. The electromagnetic field in the model is generated by a vertical magnetic dipole transmitter moving vertically along the left borehole and transmitting a signal every 10 metres. The tri-axial magnetic component receivers are located along the right borehole, deployed in the z-direction with 10 m separation. The total number of transmitter positions is 15. The total number of receivers is 15. The synthetic EM data for this model were generated using the integral equation SYSEM forward modelling code (Xiong, 1992). We use four frequencies: 10, 30, 100, and 300 Hz. The synthetic observed data were contaminated by 2% Gaussian noise and inverted using smooth and focusing regularized QL inversion. The volume between two boreholes, used for inversion, was divided into 896 cells ($8 \times 8 \times 14$ cells in $x \times y \times z$ directions), with the cells 10 $\times$ 10 $\times$ 10 m in size. Note that in order to generate good quality synthetic data, we used finer discretization for forward modelling than for inversion. Specifically, in forward modelling the conductive body was divided into 125 cells ($5 \times 5 \times 5$ cells in $x \times y \times z$ directions), with $5 \times 5 \times 5$ m cells.

In the inversion procedure we apply the grouping of the transmitters, outlined in the previous section. We divide all the transmitters into three groups: one is formed by the transmitters T1–T5, the other one is formed by the transmitters T6–T10, and the last one consists of the transmitters T11–T15, as shown in Figure 1. In this way, we achieve uniform illumination of the target from top to bottom, which increases the resolution of the inversion.
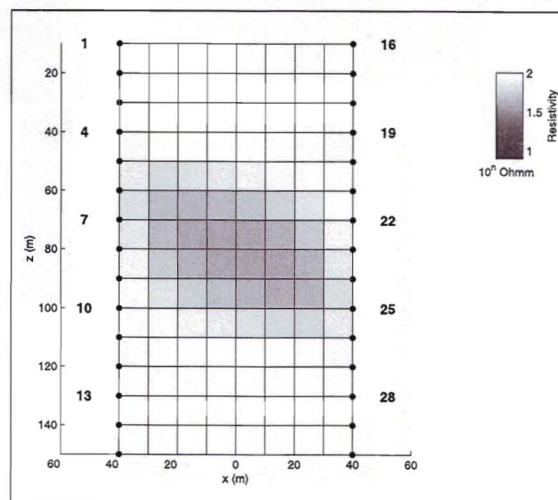

Fig. 5. A cross-section between two boreholes of the model obtained as a result of smooth inversion of the cross-hole tomographic data for Model 2. The bold numbers on the left and right of the cross-section correspond to the positions of the transmitters.

Figure 2 shows the result of the focusing inversion. It represents a vertical cross section along two boreholes. One can see very clearly an image of the conductive body in this Figure. Figure 3 shows a 3D view of the inversion result for Model 1 with a volume rendering. The cut-off level for this image is 20 ohm.m. This means that only the cells with a value of the anomalous resistivity less then 20 ohm.m are displayed. In terms of conductivity, this cut-off value represents five times the background conductivity. The selection of the cut-off value for 3D imaging is based on the analysis of the resistivity model presented in Figure 2. In practical applications, one can choose different cut-off values to produce the most suitable images for further geological interpretation.

Model 2 represents a dipping conductive body with resistivity 10 ohm.m in a 100 ohm.m homogeneous background (Figure 4). The EM field in this model is generated by two systems of vertical magnetic transmitters located in both boreholes. We also use two sets of receivers in the left and right boreholes. The synthetic data for this model for four frequencies, 10, 30, 100, and 300 Hz, were also computed using the integral equation forward modelling code. The data were contaminated by 2% Gaussian noise and inverted using smooth and focusing regularized QL inversion. We use the same grid for inversion as for Model 1.

We also apply grouping of the transmitters, outlined in the previous section, in the inversion procedure. We now divide all the transmitters and receivers into six groups: the first group is formed by transmitters T1–T5 in the left borehole and all receivers in the right borehole; the second is formed by transmitters T6–T10 in the left borehole and all receivers in the right borehole; and the third is formed by transmitters T11–T15 in the left borehole and all receivers in the right borehole. The other three groups are selected in a similar way, but with the transmitters located in the right borehole and the receivers in the left borehole. In this way, we achieve more homogeneous illumination of the target from top to bottom and from different boreholes.

Figure 5 presents the results of a traditional smooth inversion with the minimum norm stabilising functional (Zhdanov, 2002) for Model 2, the conductive dipping dike. We can see the location of the target in this image; however, the resistivity is significantly smoothed and overestimated. Figures 6 and 7 show the results of the focusing inversion for the same model. One can see that the
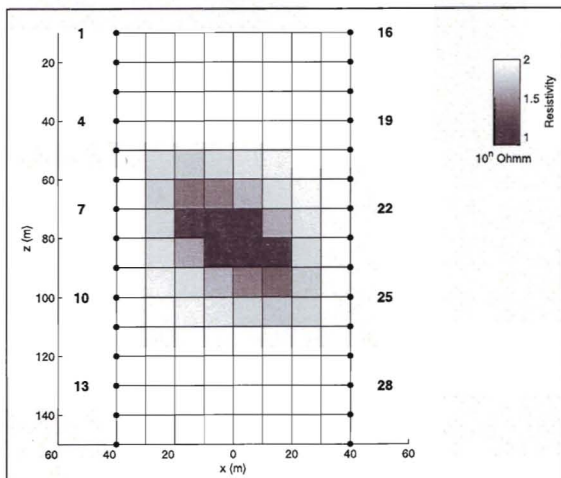
Fig. 6. A cross-section between two boreholes of the model obtained as a result of focusing inversion of the cross-hole tomographic data for Model 2. The bold numbers on the left and right of the cross-section correspond to the positions of the transmitters.
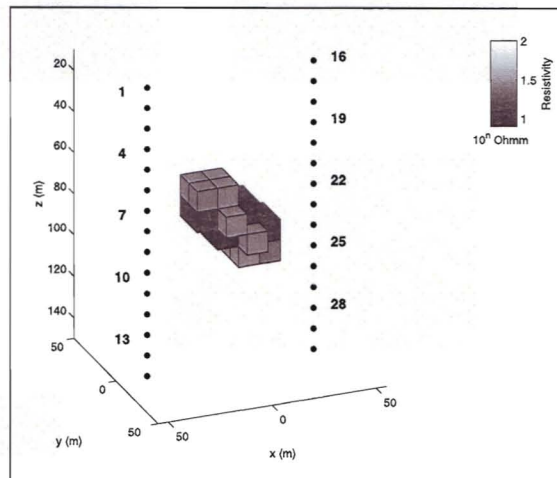

Fig. 7. A 3D view of the inversion result for Model 2 with volume rendering. The cutoff level for this image is 20 ohm.m. This means that only cells with a value of resistivity less than 20 ohm.m are displayed. The bold dots with the numbers show the transmitter locations.
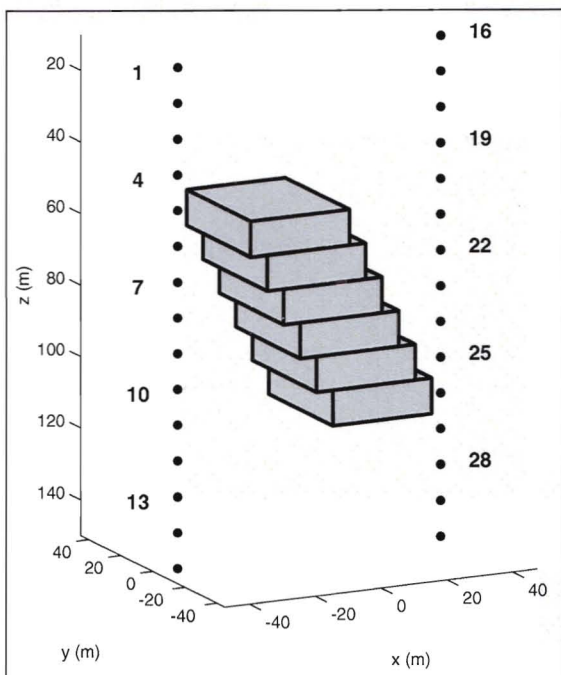

Fig. 8. Model 3, of a dipping resistive body with resistivity of 500 ohm.m in a 20 ohm.m conductive background. The bold dots with the numbers show the transmitter locations.
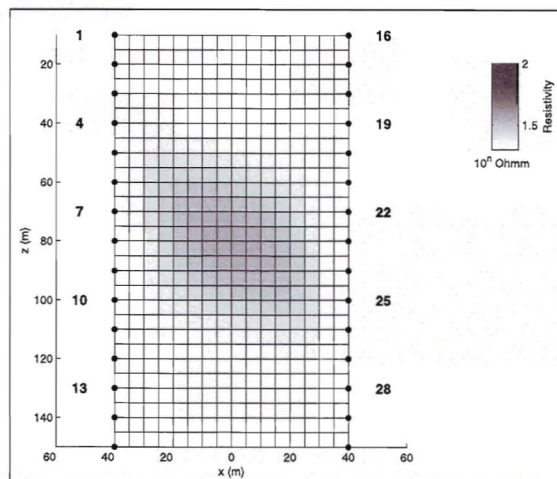

Fig. 9. A cross-section between two boreholes of the model obtained as a result of smooth inversion of the cross-hole tomographic data for Model 3. The bold numbers on the left and right of the cross-section correspond to the positions of the transmitters

image is sharp and clear, but the resistivity recovered is slightly overestimated for this conductive model. Note that the inversion was based on an approximate forward modelling solution, used with LQL approximation. In the case of a conductive target, this approximation may slightly underestimate the effect of the vortex term in the conductor, which may result in a lower conductivity of the resulting model. However, the shape and location of the target is reconstructed very well, which confirms the effectiveness and accuracy of using the LQL approximation in cross-well imaging.

Model 3 represents a dipping resistive body with resistivity of 500 ohm.m in a 20 ohm.m conductive background (Figure 8). The

cross-borehole EM survey design is similar to that considered for Model 2 with transmitters and receivers located in both boreholes. Four frequencies (10, 30, 100, and 300 Hz) have been used for computing the synthetic observed data, which were contaminated by 2% Gaussian noise. However, for this model we used a much finer discretization. The volume between the two boreholes, used for inversion, was divided into 7168 cells (16 × 16 × 28 cells in x × y × z directions), with the size of the cells 5 × 5 × 5 m.

The results of smooth and focusing inversion are shown in Figures 9 and 10. These figures represent the vertical cross-sections of the smooth model and the model with sharp boundaries, obtained by LQL inversion. Both of these models fit the data with the same accuracy of 3%. However, the images are quite different, which reflects the different nature of the smooth inversion and focusing inversion methods (Zhdanov, 2002). In mineral exploration, of course, a focused image with sharp geoelectrical boundaries is much preferred to a smoothed image. Figure 11 presents a volume rendering of the focusing inversion
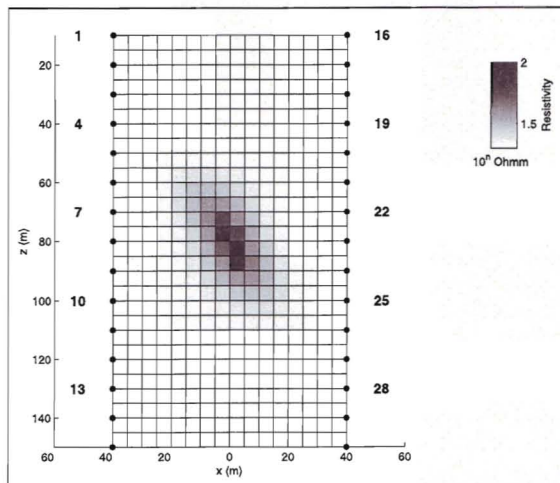
Fig. 10. A cross-section between two boreholes of the model obtained as a result of focusing inversion of the cross-hole tomographic data for Model 3. The bold numbers on the left and right of the cross-section correspond to the positions of the transmitters.
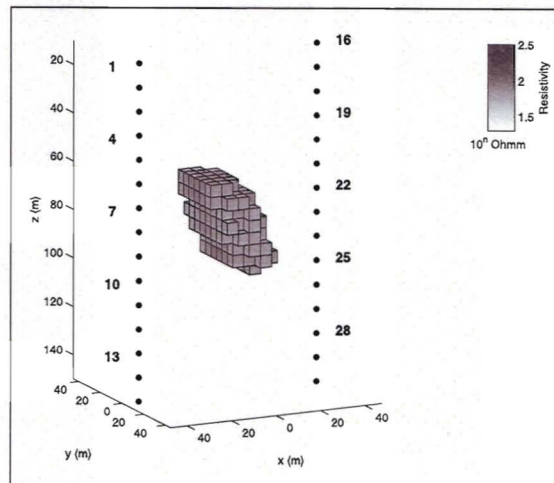

Fig. 11. A 3D view of the inversion result for Model 3 with volume rendering. The cut-off level for this image is 100 ohm.m. This means that only cells with a resistivity greater thn 100 ohm.m are displayed. The bold dots with the numbers show the transmitter locations.

result for Model 3. One can see a good resemblance to the original model in this image.

In order to check the accuracy of the LQL approximation, we conducted a numerical comparison between the observed data and predicted data computed with the rigorous IE code for the model obtained using focusing inversion. Figure 12 presents a result of such a comparison. The inversion was based on an approximate forward modelling solution with LQL approximation. However, the data shown in Figure 12 were obtained for an inverse model by rigorous forward modelling. The top panels show the real and imaginary parts of the horizontal magnetic field component H_x at frequency 100 Hz, predicted with the rigorous IE code from the inversion results. The middle panels present the real and imaginary part of the horizontal magnetic field component H_z. The bottom panels show the normalized difference (in percent) between the observed data and data predicted with the rigorous IE code. We observe an extremely good fit between the theoretical observed data and the predicted data (the maximum errors do not exceed 5%), which confirms the effectiveness and accuracy of the LQL approximation.

CONCLUSION

We have developed a new technique for 3D cross-well electromagnetic tomographic imaging. The method is based on the LQL approximation for forward modelling, which results in a fast inversion scheme.

The method incorporates both smooth regularized inversion, which generates a smooth image of the inverted resistivity, and focusing regularized inversion, producing a sharp focused image of the geoelectrical target. The practical application of the method to synthetic data demonstrates its ability to recover the resistivity, location, and shape of resistive and conductive rock formations.

Further research will be directed to examining the practical effectiveness of the method for real cross-well tomographic data.

ACKNOWLEDGEMENTS

which include Baker Atlas Logging Services, BHP Billiton World Exploration Inc., Electromagnetic Instruments, Inc., ExxonMobil Upstream Research Company, INCO Exploration, MINDECO, Naval Research Laboratory, Rio Tinto-Kennecott, Shell International Exploration and Production Inc., Schlumberger Oilfield Services, and Sumitomo Metal Mining Co.

REFERENCES

Alumbaugh, D. L., and Morrison, H. F., 1995, Theoretical and practical considerations for cross-well electromagnetic tomography assuming a cylindrical geometry: Geophysics, 60, 846–870.

Alumbaugh, D. L., and Newman, G. A., 1997, Three-dimensional massively parallel electromagnetic inversion—II. Analysis of cross-well electromagnetic experiment: Geophysical Journal International, 128, 355–363.

Newman, G. A., 1995, Cross-well electromagnetic inversion using integral and differential equations: Geophysics, 60, 899–911.

Portniaguine O., and Zhdanov, M. S., 1999, Focusing geophysical inversion images: Geophysics, 64, 874–887.

Tikhonov, A. N., and Arsenin, V. Y., 1977, Solution of ill-posed problems: V.H. Winston and Sons.

Wilt, M. J., Alumbaugh, D. L., Morrison, H. F., Becker, A., Lee, K. H., and Deszcz-Pan, M., 1995, Cross-hole electromagnetic tomography: System design considerations and field results: Geophysics, 60, 871–885.

Xiong, Z., 1992, EM modeling of three-dimensional structures by the method of system iteration using integral equations: Geophysics, 57, 1556–1561.

Zhdanov, M. S., and Fang, S., 1996a, Quasi-linear approximation in 3D EM modeling: Geophysics, 61, 646–665.

Zhdanov, M. S., and Fang, S., 1996b, 3D quasi-linear electromagnetic inversion: Radio Science, 31, 741–754.

Zhdanov, M. S., and Fang, S., 1999, 3D quasi-linear electromagnetic modeling and inversion: in Oristaglio, M. and Spies, B., eds., Three Dimensional Electromagnetics, SEG Monograph, 233–255.

Zhdanov, M. S., and Tartaras, E., 2002, Three-dimensional inversion of multitransmitter electromagnetic data based on the localized quasi-linear approximation: Geophysical Journal International, 148, 506–519.

Zhdanov, M. S., 2002, Geophysical inverse theory and regularization problems: Elsevier.

Zhou, B., and Greenhalgh, S. A., 2002, Rapid 2-D/3D cross-hole resistivity imaging using the analytic sensitivity function: Geophysics, 67, 755–769.
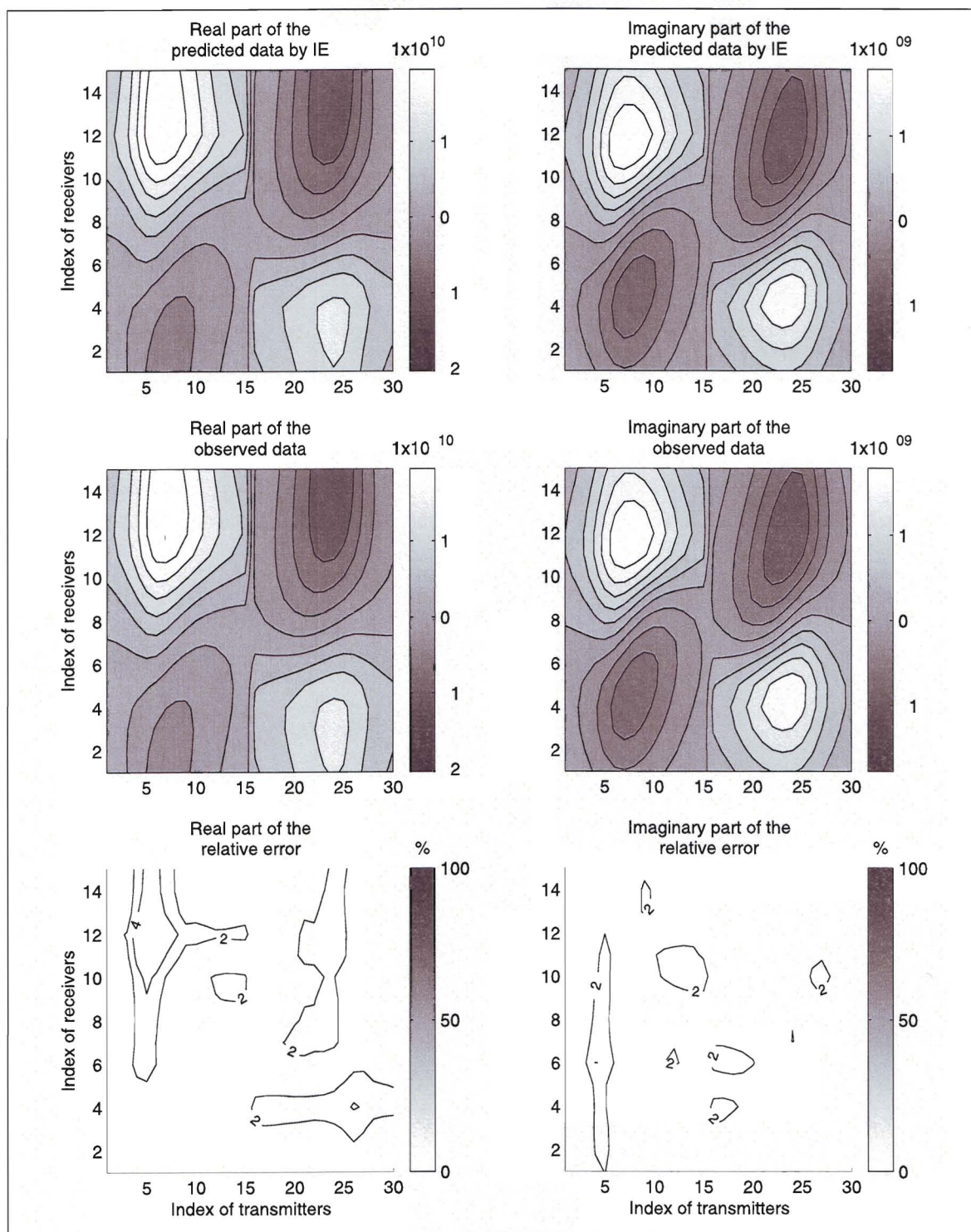
Fig. 12. A comparison between the observed data and data computed with the rigorous IE code for the inversion result for Model 3. The top panels show the real and imaginary parts of the horizontal magnetic field component Hz at frequency 100 Hz predicted with the rigorous IE code. The middle panels present the real and imaginary part of the horizontal magnetic field component Hz. The bottom panels show the normalized difference (in percent) between the observed data and data predicted with the rigorous IE code. The maps in each panel represent the data distribution in the different receivers (vertical axis) versus different transmitters (horizontal axis).